THE SEISMOLOGICAL SOCIETY OF AMERICA
400 Evelyn Ave., Suite 201
Albany, CA 94706-1375
(510) 525-5474; FAX (510) 525-7204
www.seismosoc.org

A Simple Approach to Site-Response Modeling: The Overlay Concept

by James Kaklamanos, Luis Dorfmann, and Laurie G. Baise

INTRODUCTION

Site-response analyses are used to estimate the ground motion at the surface, as a function of the properties of the soil profile and the bedrock ground motion at the base of the soil profile. The most frequently employed site-response model in engineering practice is the equivalent-linear site-response model, a frequency-domain program that is coded in the computer program SHAKE (Schnabel *et al.*, 1972; Idriss and Sun, 1992; Ordóñez, 2010). Using a large database of ground motions in the Kiban–Kyoshin network (KiK-net) of downhole arrays in Japan, Kaklamanos *et al.* (2013, 2015) found the equivalent-linear site-response model becomes inaccurate at shear strains of approximately 0.1%–0.4%. At larger strains, to model fully nonlinear behavior, site-response calculations should be performed in the time domain, which allows for a more accurate representation of the true cyclic stress–strain path. Finite-element methods are a powerful technique for modeling nonlinear site response, allowing for the representation of advanced constitutive behavior, 3D wave propagation, soil–structure interaction, and complex geometry.

The purpose of this paper is to present a simple methodology for modeling earthquake site response in any finite-element program, using an overlay model to represent nonlinear soil behavior. This paper presents a literature review of the overlay approach, the advantages of the overlay approach, practical details on its implementation in any finite-element program, how this approach may be easily extended to capture more complex behavior, and an analysis of example results using recent KiK-net data. There has been much focus in the literature on improving soil models to advance our ability to predict site response (e.g., Hartzell *et al.*, 2004; Kwok *et al.*, 2007; Phillips and Hashash, 2009). Numerous nonlinear site-response programs have been developed, including the 1D lumped-mass programs D-MOD2000 (Matasović and Ordóñez, 2010) and DEEPSOIL (Hashash *et al.*, 2011); the finite-difference program TESS (Pyke, 2000); and the finite-element programs SUMDES (Li *et al.*, 1992) and OpenSees (Ragheb, 1994; Parra, 1996; Yang, 2000; McKenna and Fenves, 2001). The overlay approach is an alternative that allows for a straightforward representation of site-response behavior in any finite-element program, giving users broad flexibility in site-response modeling. Applying parallel load-carrying elements with varying stiffness and yield stress (e.g., elastic–perfectly plastic elements), the overlay concept of Nelson and Dorfmann (1995) provides a realistic representation of the hysteretic material behavior. This approach can be used to model Masing unloading–reloading behavior (Masing, 1926) and the Bauschinger effect (a reduction in yield stress when loads are reversed [Fung, 1965]) in an efficient manner. Developing a plasticity model that correctly accounts for the Bauschinger effect can be difficult, but the overlay concept adequately represents this phenomenon without any additional modeling effort (Nelson and Dorfmann, 1995). The overlay concept can easily be extended to capture more complex behavior, such as 3D site response and cyclic hardening/softening, which are illustrated in this paper. Here, we use the general finite-element software Abaqus/Explicit (Dassault Systèmes, 2009), which has seen some prior use in seismic response studies (e.g., Sincraian and Oliveira, 2001; Balendra, 2005; Nielsen, 2006; Psarropoulos, 2009; Reyes *et al.*, 2009), but this paper is the first to directly apply the overlay concept to site response within Abaqus/Explicit.

The primary advantage of the overlay concept is its flexibility. This finite-element modeling methodology makes use of existing conventional elastoplastic material models available in any general finite-element program, allowing users broad flexibility without having to rely on complicated, program-specific models. Some nonlinear constitutive models in finite-element analyses are difficult to implement and require significant adjustments to existing numerical codes; this paper offers a simple, portable alternative that does not require any modifications to constitutive models. The overlay model can be applied with basic geotechnical data (i.e., a shear-wave velocity profile, density profile, and modulus-reduction curves), similar to the input data required for equivalent-linear analyses in SHAKE and total-stress nonlinear analyses in 1D site-response programs such as D-MOD or DEEPSOIL. For the 1D case, the predictions offered by the overlay model are similar to those from other 1D site-response programs; however, the strongest advantages of the approach may be manifested when the model is extended to capture more complex behavior; for example, 3D site response. Thompson *et al.* (2009) showed that 3D subsurface heterogeneity can significantly affect site response; the overlay model allows for an extension from 1D to 3D site response without significant additional modeling effort.

This paper is organized as follows: first, we present a review of the overlay approach, and how the elastoplastic parallel load-carrying elements can be used to replicate hysteretic

doi: 10.1785/0220140100

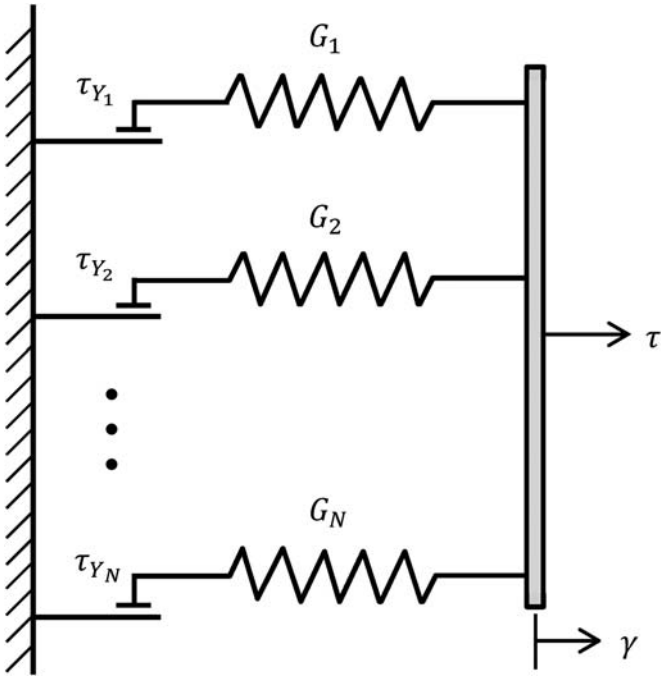

▲ **Figure 1.** Schematic representation of the 1D Iwan (1967) and Mroz (1967) material model (IM67) composed of elastoplastic springs in parallel.

behavior. Then, we present a novel derivation of the shear moduli and yield stresses of the individual overlay elements. Next, we provide practical, explicit details on how the overlay model may be implemented in a finite-element analysis for 1D site response. As an example, we present and compare results of site-response analyses for a strong ground motion at station IWTH08 (National Earthquake Hazards Reduction Program [NEHRP] site class D) in the KiK-net of downhole arrays in Japan. We choose the IWTH08 site for our model validation because Thompson *et al.* (2012) classifies IWTH08 as a good site for 1D validation studies of site-response models. The 1D model validation is a necessary step prior to 3D model implementation, and the comprehensive details on the 1D implementation of the overlay concept in this paper provide a pathway for modeling more advanced material behavior. Finally, we briefly outline how the overlay modeling approach can be used to simulate more complex behavior: (a) 3D site response and (b) cyclic hardening and cyclic softening, illustrating the flexibility of the overlay approach.

OVERLAY MODELING CONCEPT

As described by Dorfmann and Nelson (1995) and Nelson and Dorfmann (1995), an overlay model uses parallel load-carrying elements with varying stiffness and yield stress to replicate the behavior of a backbone stress–strain curve. To represent overlay elements in a finite-element model, the user defines a number of finite elements and assigns each of them identical node numbers. Because the parallel elements have equal displacement components on the element nodes, the N elements have identical strain components: $\epsilon_{ij} = (\epsilon_{ij})_1 = ... = (\epsilon_{ij})_N$. The total stress corresponding to a given strain is additively decomposed: $\sigma_{ij} = (\sigma_{ij})_1 + ... + (\sigma_{ij})_N$. This simple modeling strategy accurately accounts for hysteretic behavior, representing the Bauschinger effect and extended Masing behavior in a straightforward manner.

When parallel load-carrying elements are defined using the overlay concept in a finite-element model, the resulting behavior is consistent with a general class of material models originally conceived by Iwan (1967) and Mroz (1967), termed the IM67 model. Iwan (1967) and Mroz (1967) represented the stress–strain response of a material using a set of elastoplastic springs connected in parallel. Each element is composed of a linear spring with shear modulus G_i and a Coulomb friction element with yield stress τ_{Y_i}, as illustrated in Figure 1 for the 1D case. The IM67 model has been applied in a number of soil dynamics studies (typically using finite-difference programs), first by Joyner and Chen (1975) and Joyner (1977) in the finite-difference program NONLI3. The finite-difference programs NERA (Bardet and Tobita, 2001) and NOAHW (Hartzell *et al.*, 2004) use IM67 as their primary constitutive model and have been employed by a number of users (e.g., Hartzell *et al.*, 2002; Liu *et al.*, 2006; Irsyam *et al.*, 2008; Sandron *et al.*, 2011). The IM67 model was modified by Yang (2000) and Elgamal *et al.* (2003) and incorporated as a constitutive model in the OpenSees finite-element platform (McKenna and Fenves, 2001). The IM67 model is a general constitutive model, and the overlay approach is a convenient alternative mechanism for representing the IM67 model using finite-element programs, by specifying N parallel elements with the same nodal points.

A basic illustration of the stress–strain response for the case of $N = 3$ parallel elements is shown in Figure 2. The total stress–strain curve of the material is given by the addition of the stresses in the individual parallel elements, which are all subject to the same deformation. The stress–strain behavior of an individual element (denoted i) is elastic with shear modulus G_i for strains less than γ_i and becomes perfectly plastic with yield stress τ_{Y_i} for strains exceeding γ_i. The stress–strain behavior of the material is defined by a sequence of yield points that occur at increasingly higher strain levels, replicating the behavior of the backbone curve $\tau = f(\gamma)$. Specifically, the total shear stress τ for a given shear strain γ is represented by the sum of elastic and plastic components:

$$\tau(\gamma) = \sum_{i=1}^{n} G_i\gamma + \sum_{i=n+1}^{N} \tau_{Y_i}, \tag{1}$$

in which n is the number of elements that remain elastic up to strain γ and N is the total number of elements. The shear modulus of the material is equal to the sum of the shear moduli of the individual elements. For increasing strains, more of the parallel elements are forced to yield, and the load must be carried by a smaller number of elastic elements. As strains increase,

the shear stiffness of the material becomes successively smaller. When the final element reaches the elastic limit, the maximum load-carrying capacity of the material is reached, and no further increase in load is possible. The yield criterion associated with the overlay model is that of multi-yield-surface J_2 (or von Mises) plasticity (Iwan, 1967; Mroz, 1967).

By increasing the number of parallel load-carrying elements, the approximation of the numerical method improves. We performed a sensitivity analysis on the number of overlay elements N required to adequately represent the predicted response and amplification spectra of multiple KiK-net ground motions (using values of N from 3 to 50), we find that site-response predictions are nearly identical for $N > 20$, and there are no significant differences when as low as $N = 10$–15 overlay elements are used. However, the differences are more significant for $N < 10$. The selection of an appropriate number of overlay elements represents a balance between prediction accuracy and computational cost.

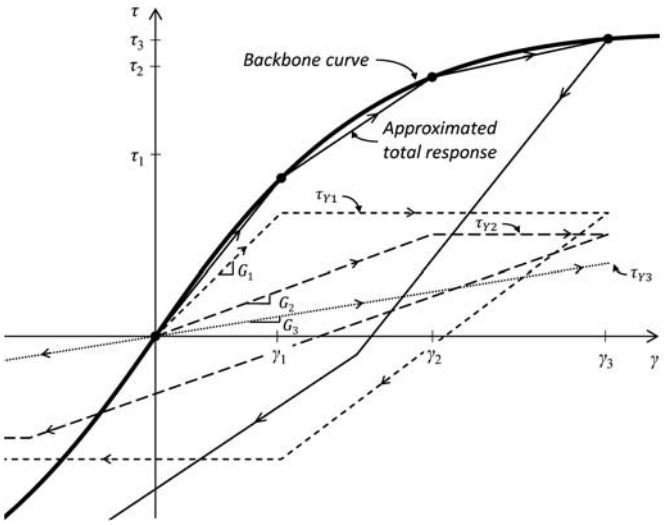

▲ **Figure 2.** Stress–strain behavior for $N = 3$ elastoplastic elements in parallel. The dashed lines indicate the stress–strain behavior of each element (with individual shear moduli G_i and yield stresses τ_{Y_i} labeled), and the solid lines indicate the total stress–strain response of the material. The backbone curve is also shown. In the illustration, the material is loaded to a maximum strain of γ_3, but it could be loaded to any strain level. For strains greater than γ_3, the material would behave in a perfectly plastic manner.

MATERIAL PARAMETERS AND DAMPING

To model nonlinear soil behavior, the user must specify N data points of a 1D backbone stress–strain curve $\tau = f(\gamma)$, which lead to N parallel elements. The general multilinear stress–strain equation is

$$\tau(\gamma) = \begin{cases} (G_1 + G_2 + \ldots + G_N)\gamma & \text{for } 0 \le \gamma \le \gamma_1 \\ \tau_{Y1} + (G_2 + \ldots + G_N)\gamma & \text{for } \gamma_1 \le \gamma \le \gamma_2 \\ \vdots & \\ \tau_{Y1} + \ldots + \tau_{Y(i-1)} + (G_i + \ldots + G_N)\gamma & \text{for } \gamma_{i-1} \le \gamma \le \gamma_i \\ \tau_{Y1} + \ldots + \tau_{Y(i-1)} + \tau_{Yi} + (G_{i+1} + \ldots + G_N)\gamma & \text{for } \gamma_i \le \gamma \le \gamma_{i+1} \\ \vdots & \\ \tau_{Y1} + \ldots + \tau_{Y(N-1)} + G_N\gamma & \text{for } \gamma_{N-1} \le \gamma \le \gamma_N \\ \tau_{Y1} + \ldots + \tau_{Y(N-1)} + \tau_{YN} & \text{for } \gamma \ge \gamma_N \end{cases}. \tag{2}$$

From the backbone curve, we present a novel, alternative algorithm for determining the shear moduli G_i and yield stresses τ_{Y_i}, $i = 1, \ldots, N$, of the N parallel elements, summarized and derived in greater detail by Kaklamanos (2012) and Kaklamanos *et al.* (2014). Each inequality in equation (2) is closed, meaning that at the breakpoints (γ_i, τ_i), $i = 1, \ldots, N$, two possible stress–strain equations are valid: (1) the equation for the preceding linear segment and (2) the equation for the successive linear segment. This equivalence is possible because the yield stresses τ_{Y_i} are related to the shear moduli G_i by the equation $\tau_{Y_i} = G_i\gamma_i$; element i switches from elastic to perfectly plastic at strain γ_i. Applying equation (2) twice at each of the N breakpoints, we obtain a system of $2N$ equations in $2N$ unknowns, which can then be converted into matrix form and solved for the material parameters as follows:

$$G_1 = \frac{\tau_1}{\gamma_1} - \frac{\tau_1 - \tau_2}{\gamma_1 - \gamma_2}, \tag{3}$$

$$G_i = \frac{\tau_{i-1} - \tau_i}{\gamma_{i-1} - \gamma_i} - \frac{\tau_i - \tau_{i+1}}{\gamma_i - \gamma_{i+1}}, \qquad i = 2, \ldots, N-1, \tag{4}$$

$$G_N = \frac{\tau_{N-1} - \tau_N}{\gamma_{N-1} - \gamma_N}, \tag{5}$$

$$\tau_{Y1} = \frac{\tau_2\gamma_1 - \tau_1\gamma_2}{\gamma_1 - \gamma_2}, \tag{6}$$

$$\tau_{Yi} = \frac{\tau_{i+1}\gamma_i - \tau_i\gamma_{i+1}}{\gamma_i - \gamma_{i+1}} - \frac{\tau_i\gamma_{i-1} - \tau_{i-1}\gamma_i}{\gamma_{i-1} - \gamma_i}, \qquad i = 2, ..., N-1, \tag{7}$$

and

$$\tau_{YN} = \tau_N - \frac{\tau_N\gamma_{N-1} - \tau_{N-1}\gamma_N}{\gamma_{N-1} - \gamma_N}. \tag{8}$$

To apply the overlay model in a finite-element analysis, we must specify the densities of the individual overlay elements ρ_i, $i = 1, ..., N$, as the total material density (ρ) divided by the number of overlay elements: ρ/N. The density ρ may be calculated from seismic velocity data using a procedure such as that of Boore (2007). Because seismic velocities usually increase with depth throughout a soil profile, the density will increase with depth as well. Many general finite-element codes (such as Abaqus/Explicit) require input in terms of Young's modulus E, Poisson's ratio μ, and plastic yield stress σ_Y. Poisson's ratio μ may be computed from seismic velocity data by the relation

$$\mu = (V_P^2 - 2V_S^2)/[2(V_P^2 - V_S^2)], \tag{9}$$

in which V_S is S-wave velocity and V_P is P-wave velocity. For simplicity, we use $\mu = \mu_1 = ... = \mu_N$ for each of the parallel elements. Using G_i and μ_i, the Young's moduli E_i of the elements can then be determined: $E_i = 2G_i(1 + \mu_i)$. From the J_2 plasticity criterion, the plastic yield stress σ_Y is obtained as

$$\sigma_Y = \sqrt{\frac{1}{2}[(\sigma_x - \sigma_y)^2 + (\sigma_y - \sigma_z)^2 + (\sigma_z - \sigma_x)^2 + 6(\tau_{xy}^2 + \tau_{yz}^2 + \tau_{xz}^2)]}. \tag{10}$$

For pure shear (the state of stress in a 1D site-response analysis), the only nonzero value is the yield shear stress, $\tau_{xz} = \tau_Y$. Simplifying equation (10), we have $\sigma_{Y_i} = \sqrt{3}\tau_{Y_i}$, the plastic yield stress to be computed for each parallel element.

Nonlinear site-response models generally have two types of damping: (1) hysteretic damping, which is associated with energy dissipation within hysteresis loops and (2) viscous (velocity-proportional) damping, which is associated with dashpots embedded within the material elements. Hysteretic damping (or material damping) is governed by the unloading–reloading rules of the material model; for example, Masing behavior would dictate the area inside the closed hysteresis loops for the 1D incorporation of overlay elements. An equation for the hysteretic damping ratio (ξ) for a backbone curve composed of N linear segments, defined by the points (γ_i, τ_i), $i = 1, 2, ..., N$, is

$$\xi(\gamma_a) = \frac{2}{\pi}\left[\frac{\sum_{i=2}^{a}(\tau_i + \tau_{i-1})(\gamma_i - \gamma_{i-1})}{\gamma_a\tau_a} - 1\right] \tag{11}$$

(Ishihara, 1996; Kaklamanos, 2012). The sum is over a points ($1 \le a \le N$), so the damping ratio can be evaluated for different strain amplitudes, from γ_1 to γ_N. Because there is little hysteretic damping at small strains, many nonlinear site-response codes include some level of viscous damping to maintain some damping at small strains. In time-domain analyses, Rayleigh damping (Rayleigh and Lindsay, 1945) is the usual mechanism for incorporating viscous damping.

FINITE-ELEMENT MODEL

The finite-element analysis framework summarized here is a 1D total stress analysis, representing vertically propagating shear waves through horizontal layers of soil and rock; extensions to more advanced behavior are described in the following sections. A schematic of the finite-element model for 1D site response is shown in Figure 3. The model is a rectangular prism composed of eight-node 3D brick elements with unit width in the x and y directions and total height H in the z direction, in which H is the thickness of the geologic profile. The soil column is divided into sublayers composed of elements with heights h_i selected to account for the transmission of high-frequency energy: there need to be a sufficient number of elements per wavelength in the direction of wave propagation. A general rule of thumb for finite-difference and finite-element models is to specify 10 grid points per wavelength (Alford *et al.*, 1974). Therefore, the maximum frequency f_{max} of shear waves propagated through the model is $V_S/(10h)$, in which V_S and h are the S-wave velocity and thickness of the element, respectively. For a given f_{max}, the upper bound on the allowable element thickness is $h \le V_S/(10f_{max})$. We select $f_{max} = 25$ Hz for our analyses, because little seismic energy is transmitted at frequencies above this range. This element thickness requirement leads to progressively thinner elements near the top of the soil profile, in which V_S is smaller. The upper layers have a nonlinear response, and the lower layers (below the soil–bedrock interface) are modeled as linear elastic.

The loading is applied in the x direction, and all nodes are restrained in the y and z directions to represent vertically propagating shear waves. The output from the site-response analysis is typically the horizontal acceleration at the ground surface, as well as shear stresses and strains at various locations throughout the soil profile. The loading and boundary conditions at the bottom of the model are specified in one of two ways, depending on the type of recorded input motion being used. As summarized in detail by Kaklamanos (2012) and Kwok *et al.* (2007), rigid boundaries are used when the input motion is taken from a downhole recording at a vertical array site, and absorbent (or "quiet") boundaries, representing an elastic base, are used when the input motion is taken from an outcrop recording. For the case of a downhole recording (requiring a rigid boundary), the input motion may be speci-

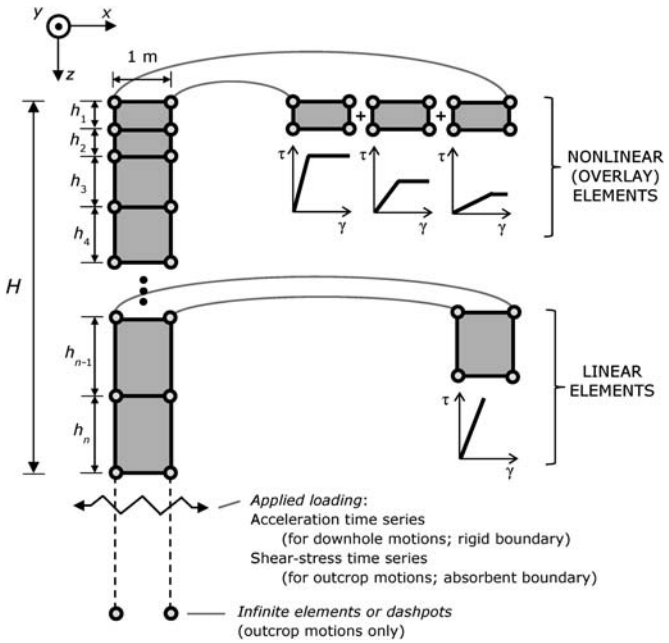

▲ **Figure 3.** A 1D finite-element model for site-response calculations, illustrating the coordinate convention, applied loading, and implementation of overlays. The model has unit thickness in the *y* direction (out of the plane of the page), and there is an analogous set of nodes 1 m in the *y* direction from the nodes shown. At the bottom of the model, infinite elements or dashpots are only used when the input motion is obtained from an outcrop recording. The upper layers, representing soil, are modeled by overlays (nonlinear behavior), and the lower layers, representing rock, are modeled by single elements (linear behavior).

fied as is; the acceleration time series is directly specified as a boundary condition at the nodes corresponding to the base of the soil column. For the case of an outcrop recording (requiring an absorbent boundary), the input motion is applied as a stress wave at the bottom nodes, and the absorbent boundary is constructed using either infinite elements or viscous dashpots connected to the bottom nodes. Using the methodology of Lysmer and Kuhlemeyer (1969) and Joyner and Chen (1975), the input motion is expressed as $\tau(t) = \rho_r V_{S_r} V_{\text{outcrop}}(t)$, in which $\tau(t)$ is the shear–stress time series applied at the absorbent boundary, ρ_r is the density of the basement rock, V_{S_r} is the shear-wave velocity of the basement rock, and $V_{\text{outcrop}}(t)$ is the velocity time series of the input ground motion, obtained from a rock outcrop recording at the ground surface. The absorbent boundary allows for energy to be transmitted into the underlying half-space.

1D SITE-RESPONSE VALIDATION

In this section, we present the results of a site-response analysis at station IWTH08 in KiK-net, a collection of surface–downhole arrays in Japan (Aoi *et al.*, 2000; Okada *et al.*, 2004; see Data and Resources). The downhole ground-motion recording is used as an input to a site-response model, and

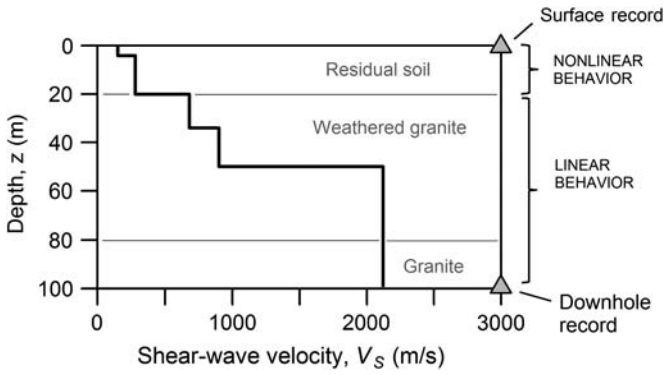

▲ **Figure 4.** Profile of shear-wave velocities and geologic layers at KiK-net station IWTH08.

the surface ground motion predicted by the site-response model can be compared with the recorded ground motion at the surface. Station IWTH08 (latitude 40.2658°, longitude 141.7867°) is located in Kuji, in Iwate prefecture on northern Honshu island. The site consists of 83 m of weathered granite over competent granite, has an average shear-wave velocity of $V_{S30} = 305$ m/s over the top 30 m of the subsurface, and is an NEHRP class D site (Building Seismic Safety Council [BSSC], 1998). Figure 4 presents the shear-wave velocity profile and geologic summary obtained from the KiK-net website (see Data and Resources). Because of the low V_S values in the upper 20 m, we assume that the upper 20 m is composed of residual soil.

As a representative example to validate the approach in 1D, we compare site-response model predictions for a strong event recorded at station IWTH08: the 24 July 2008 **M** 6.8 Iwate event. According to the Thompson *et al.* (2012) classification scheme, IWTH08 adequately meets the assumptions of 1D site response and therefore is an ideal site for validating 1D nonlinear site-response models. Linear and equivalent-linear site-response calculations are performed using the program SHAKE2000 (Schnabel *et al.*, 1972; Idriss and Sun, 1992; Ordóñez, 2010), with the modulus-reduction and damping curves of Zhang *et al.* (2005). Fully nonlinear site-response calculations are performed for the 1D case using the general finite-element program Abaqus/Explicit (Dassault Systèmes, 2009), following the modeling procedure described in this paper. We also compare results from the 1D nonlinear site-response program DEEPSOIL (Hashash *et al.*, 2011). In both programs, the nonlinear stress–strain behavior of the upper 20 m is characterized using backbone curves generated from the Zhang *et al.* (2005) modulus-reduction curves; for the bottom 80 m, the rock material is assumed to exhibit linear stress–strain behavior for all analyses. In Abaqus/Explicit, we use $N = 20$ overlay elements to model the stress–strain response at each depth.

Figure 5 provides detailed comparisons of the site-response model predictions: time series, stress–strain loops, response spectra, and profiles of maximum shear strain. The plots show large differences between the linear, equivalent-linear, and nonlinear site-response models. As illustrated in Figures 5c and 5e, the linear site-response model greatly overpredicts the level of

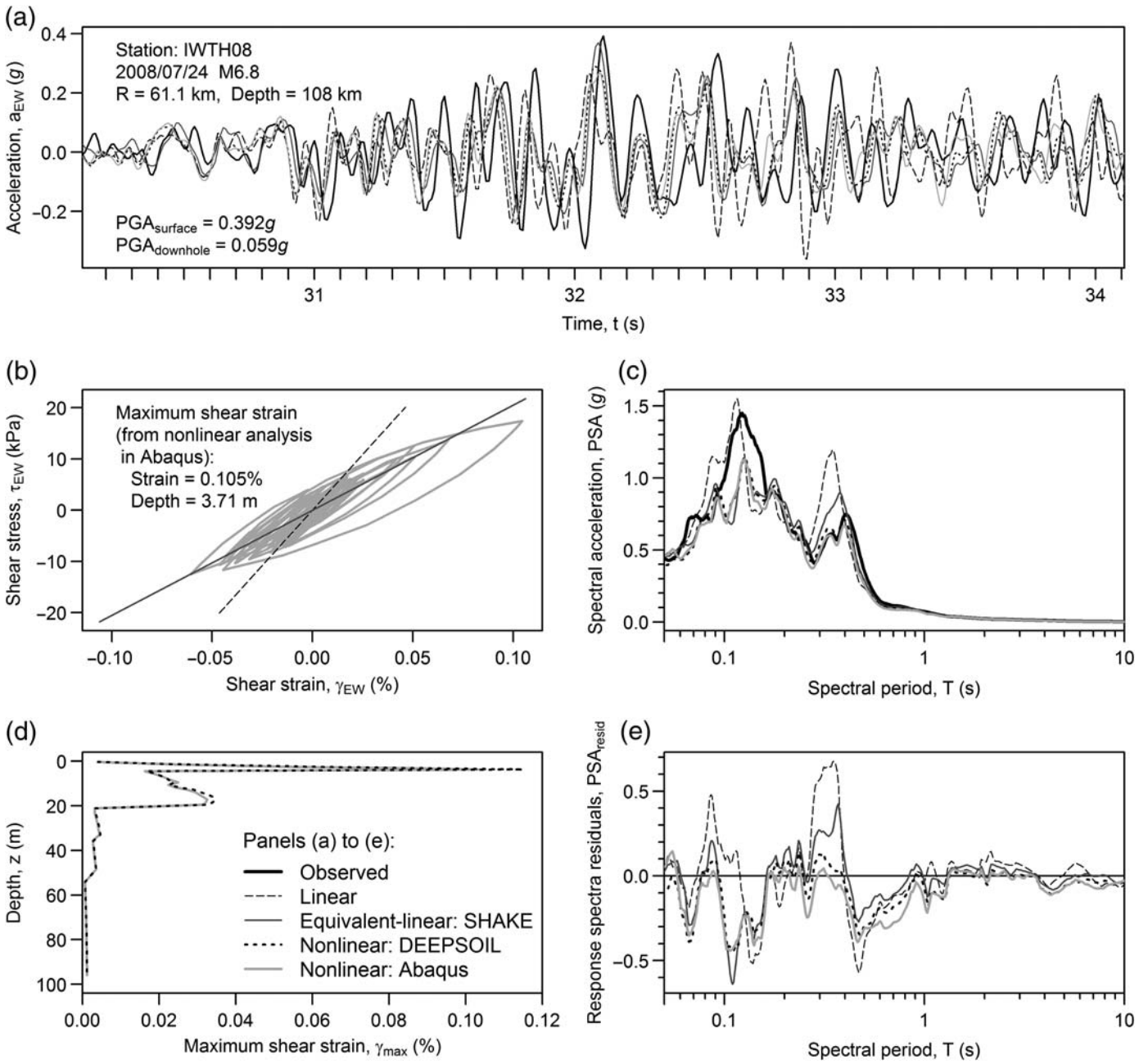

▲ **Figure 5.** Detailed comparison of ground-motion predictions for the **M** 6.8 Iwate event of 24 July 2008, recorded at station IWTH08: (a) observed and predicted surface acceleration time series (east–west component) centered in a 5 s window around the time of the absolute maximum acceleration; (b) predicted stress–strain loops (east–west component) at the depth corresponding to the maximum shear strain in the profile; (c) observed and predicted 5% damped pseudoacceleration response spectra (PSA) for the geometric mean surface ground motions; (d) profiles of maximum shear strain versus depth; and (e) residuals of the observed and predicted response spectra in (c), computed as $PSA_{resid} = \ln(PSA_{obs}) - \ln(PSA_{pred})$.

ground motion, and this overprediction is especially severe at spectral periods in the 0.3–0.4 s range, where the fundamental peak of the linear site-response theoretical transfer function is located (0.36 s). Near this fundamental peak, the equivalent-linear model is able to improve the prediction, but the nonlinear models more closely match the observations. The stress–strain curves in Figure 5b illustrate the weaknesses of the linear and equivalent-linear models; the fully nonlinear site-response analyses, on the other hand, allow for a more accurate representation of the true cyclic stress–strain path. No significant differences are observed between the model predictions of the two nonlinear site-response programs, although Figure 5e shows that in the range of the fundamental peak of the amplification spectrum (near 0.3 s), the nonlinear site-response predictions in Abaqus/Explicit are slightly less biased than those from DEEPSOIL.

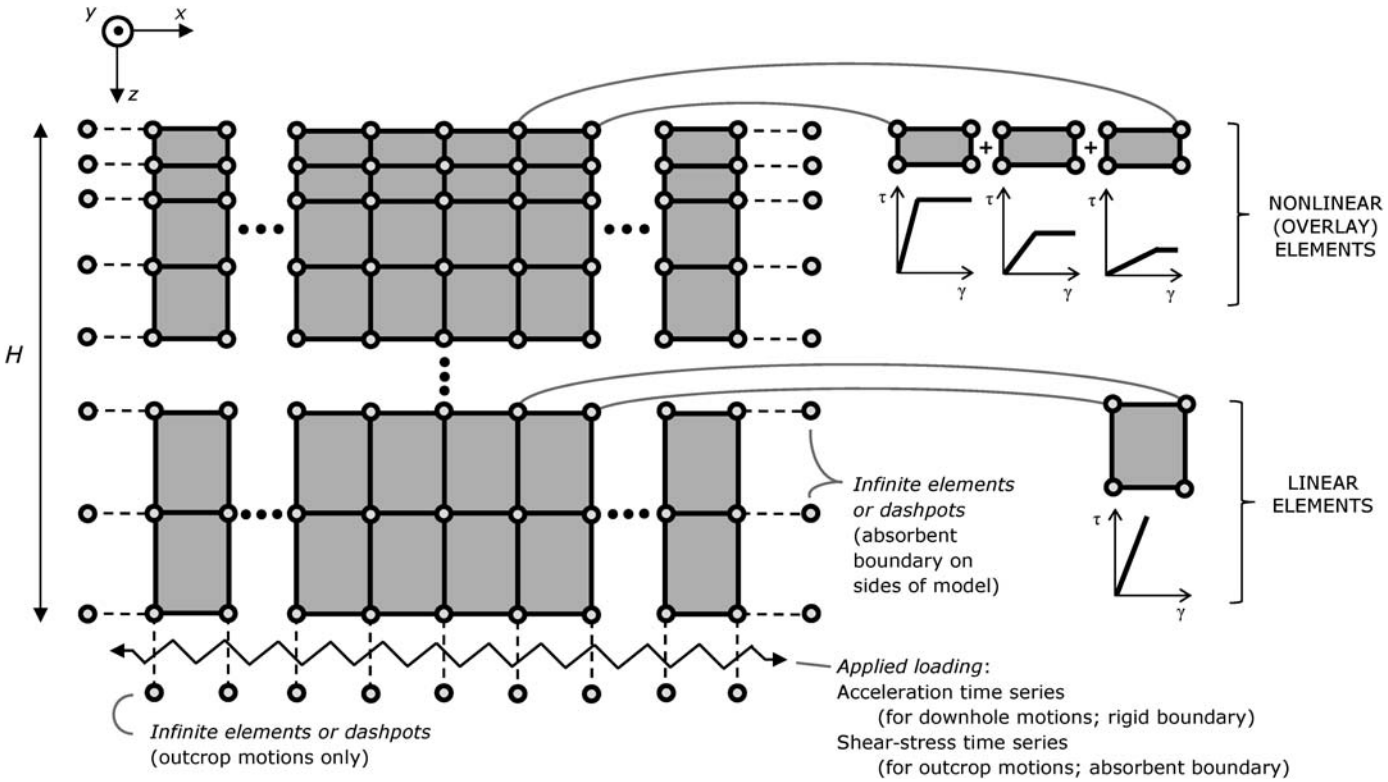

▲ **Figure 6.** Generalization of the overlay model to represent 3D site-response behavior. The model is symmetric in the *x* and *y* directions (the *y* direction is out of the plane of the page and not shown). On the sides of the model, infinite elements or dashpots are required to establish an absorbent boundary scheme. At the bottom of the model, like the 1D case, infinite elements or dashpots are used when the input motion is obtained from an outcrop recording.

More detailed validations and comparisons of the nonlinear site-response overlay model, along with other linear, equivalent-linear, and nonlinear site-response models, were presented for multiple KiK-net sites and ground motions in Kaklamanos (2012) and Kaklamanos *et al.* (2015). Equivalent-linear and nonlinear site-response predictions were generally found to be similar, with nonlinear site-response models showing a statistical improvement over the simpler models for shear strains $> 0.05\%$. In the aggregate, the nonlinear overlay model in Abaqus/Explicit displayed slightly lesser bias than predictions from SHAKE2000 and DEEPSOIL at short spectral periods (< 0.2 s). All model predictions were extremely sensitive to the selection of the modulus reduction and damping relationship; the Zhang *et al.* (2005) curves were found to have the strongest goodness-of-fit.

SIMULATION OF MULTIDIMENSIONAL SITE RESPONSE

Besides its portability to different finite-element programs, one of the advantages of the overlay model is that it can be easily adapted to model more complex behavior, such as 2D or 3D site response or cyclic hardening and softening. Inherent to a 1D site-response analysis, it is assumed that (1) the medium consists of laterally constant layers overlying a nonattenuating half-space, (2) wavefronts are planar, and (3) only the *SH* wave is modeled. Compounding factors such as basin waves, path effects, soil heterogeneity, nonvertical incidence, and poorly constrained soil properties can greatly reduce the accuracies of 1D site-response models (Baise *et al.*, 2011; Kaklamanos *et al.*, 2013). The flexibility of the overlay concept allows for 3D site response to be incorporated in a straightforward manner. As described by Dawson *et al.* (2013) in their application to the finite-difference program FLAC, the modeling principle of parallel plasticity (illustrated in Fig. 1 for the 1D case) also can be applied in 2D or 3D. This means that the overlay concept can also be directly applied in a 2D or 3D finite-element analysis to represent the IM67 material model.

Figure 6 is a schematic of a multidimensional finite-element model for site response. The boundary conditions on the bottom of the model are the same as those for the 1D case; the boundary conditions on the sides of the model are absorbent, allowing energy to be transmitted beyond the model in the *x* and *y* directions. One component of horizontal ground motion may be input at the base in the *x* direction, or multiple components may be applied simultaneously to measure the response to multiaxial base excitation. The 3D framework may be easily simplified to model 2D site response by specifying a model width of one element in the *y* direction and restraining the nodes in that direction. To capture geologic heterogeneities

in the subsurface, the seismic velocities may be generated by spatially correlated random fields, using the procedure described, for example, by Thompson *et al.* (2009). The data required are one or more measured V_S profiles, along with an assumed spatial correlation structure for shear-wave velocity. Further work is needed to quantify the gains in prediction accuracy obtained by accounting for 3D site-response effects.

SIMULATION OF CYCLIC HARDENING AND SOFTENING

With minor adjustments, an extension of the overlay approach allows for cyclic hardening and softening to be represented in the model. Using Masing behavior, the backbone stress–strain curve is assumed to be constant throughout the duration of the loading. However, there may be situations in which this assumption is unrealistic (e.g., long duration, large-amplitude events), when the backbone curve should be allowed to change with a progressive number of loading cycles. Under cyclic hardening behavior, the backbone curve experiences an increase in shear modulus when subjected to repeated cyclic loads. Cyclic hardening behavior may be observed, for example, in unsaturated sands when significant volume change occurs due to rearrangement of soil particles (Lee *et al.*, 2009). Under cyclic softening behavior, on the other hand, the backbone curve experiences a decrease in shear modulus when subjected to repeated cyclic loads. Cyclic softening behavior may occur, for example, in saturated sand and clay due to the development of pore water pressures.

Modeling options for cyclic hardening and softening are not available in all site-response programs or may require substantial adjustment to existing codes. However, a simple adjustment to the overlay element definition allows for cyclic hardening or softening to be included in the model. In the standard overlay model, the stress–strain behavior of an individual element is elastic–perfectly plastic. To incorporate cyclic hardening or softening, the horizontal slope of the plastic portion of the stress–strain curve is changed to a positive slope $H > 0$ (to model cyclic hardening behavior) or a negative slope $H < 0$ (to model cyclic softening behavior), as shown in Figure 7. The stress–strain curves for three materials (elastic–perfectly plastic, cyclic hardening, and cyclic softening) are shown in panels a, b, and c, respectively (for $N = 3$ overlay elements as an example), and the resulting cyclic hysteresis loops are shown in panels d, e, and f, respectively (using a larger number of overlay elements, so that the curves are less coarse). In Figures 7b and 7c, the slopes of the plastic components H_i are assumed to be equal for each of the $N = 3$ cyclic hardening and softening elements, although this does not need to be the case. The materials are loaded to four successively larger strain levels. The cyclic hardening behavior in Figure 7e is similar to the behavior represented in Lee *et al.* (2009), which modified the IM67 material model for cyclic hardening behavior of sand. The cyclic softening behavior in Figure 7f is similar to hysteresis loops from constitutive models, allowing stiffness degradation due to excess pore pressure generation, such as Matasović and Vucetic (1993) for sands and Matasović and Vucetic (1995) for clays. To implement cyclic hardening and softening using overlays, the user would first solve for the shear moduli and yield stresses of the overlay elements (i.e., determine the $2N$ unknown parameters using equations 3–8) and then determine the appropriate plastic modulus H from cyclic test data.

SUMMARY

In this paper, we presented a simple methodology for modeling earthquake site response using the overlay concept within a general finite-element framework. The Iwan (1967) and Mroz (1967) material model, which has been applied to soil dynamics in a number of finite-difference programs, may be conveniently represented using overlays in finite-element programs without requiring any specific built-in constitutive models. The overlay model for earthquake site response has a number of advantages: the approach is extremely flexible, can be implemented in nearly any existing finite-element code (including general codes not specifically designed for site response), and can be easily adapted to model more complex behavior (such as cyclic hardening and softening, and 2D and 3D site response). Explicit details have been provided on the implementation of the overlay model, with the hope that users will be able to incorporate site response into existing finite-element programs for other applications, such as wave propagation simulations or soil–structure interaction studies. The 1D validation at KiK-net site IWTH08 showed that the overlay model is able to accurately predict surface ground motions and can be extended to other sites that require 3D complexity in stratigraphy or heterogeneity of soil properties.

DATA AND RESOURCES

We obtained the earthquake ground-motion records, seismic velocity profiles, and geologic profiles for station IWTH08 using the Kiban-Kyoshin network (KiK-net) database at http://www.kyoshin.bosai.go.jp/ (last accessed October 2014). To compute the 5% damped pseudoacceleration response spectra from the acceleration time series, we used the Boore (2008) FORTRAN programs. The linear and equivalent-linear site-response calculations were performed using the site-response program SHAKE2000 (Schnabel *et al.*, 1972; Idriss and Sun, 1992; Ordóñez, 2010). The nonlinear site-response calculations were performed using the site-response program DEEPSOIL (Hashash *et al.*, 2011) and the finite-element program Abaqus/Explicit (Dassault Systèmes, 2009); linear analyses were also performed in these programs as a validation step.

ACKNOWLEDGMENTS

This research was supported under National Science Foundation (NSF) Grant Number 1000210; we gratefully acknowledge this support. We are grateful for detailed reviews and feedback from Nori Nakata (Stanford University), an anonymous

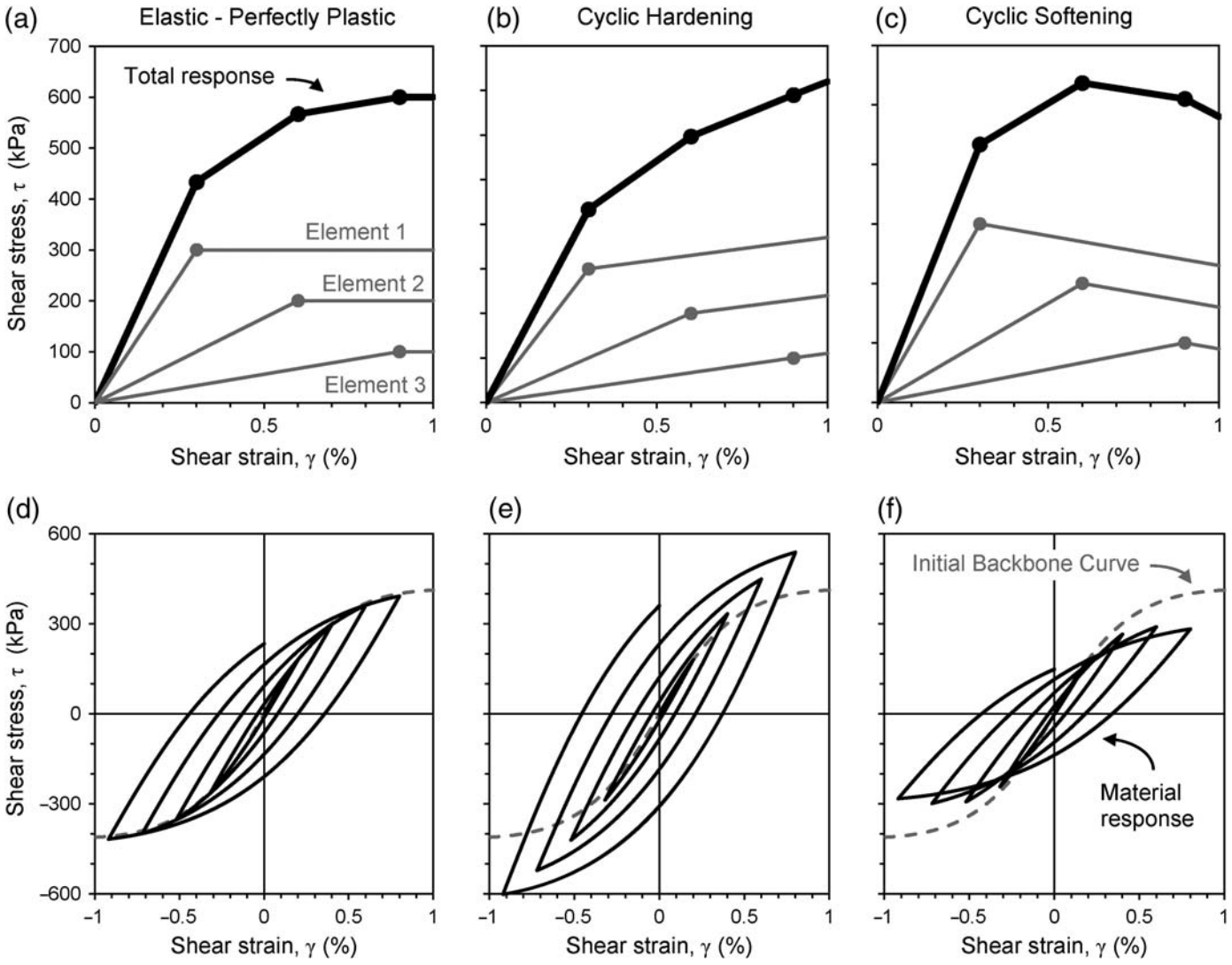

▲ **Figure 7.** Generalization of the overlay model to represent cyclic hardening and softening behavior. The first row displays the stress–strain curves for the (a) elastic–perfectly plastic material, (b) cyclic hardening material, and (c) cyclic softening material, using $N = 3$ overlay elements as an example. The second row (d–f) displays the corresponding hysteresis loops when the materials are loaded to four successively larger strain levels, using a larger number of overlay elements so that the curves are less coarse.

reviewer, and the associate editor, whose comments greatly improved the quality of this manuscript. Eric Thompson (San Diego State University) offered important contributions to this work, and David M. Boore (U.S. Geological Survey) provided helpful comments on this manuscript. We also thank Adrian Rodriguez-Marek (Virginia Tech) for making the finite-element modeling work of his former student, Surendran Balendra, available to us.

REFERENCES

Alford, R. M., K. R. Kelley, and D. M. Boore (1974). Accuracy of finite difference modeling of the acoustic wave equation, *Geophysics* **39,** 834–842.

Aoi, S., K. Obara, S. Hori, K. Kasahara, and Y. Okada (2000). New Japanese uphole–downhole strong-motion observation network: KiK-net, *Seismol. Res. Lett.* **72,** 239.

Baise, L. G., E. M. Thompson, J. Kaklamanos, and L. Dorfmann (2011). Complex site response: Does one-dimensional site response work? *4th IASPEI (International Association of Seismology and Physics of the Earth's Interior)/IAEE (International Association of Earthquake Engineering) International Symposium on the Effects of Surface Geology on Seismic Motion (ESG4)*, Santa Barbara, California, 23–26 August 2011.

Balendra, S. (2005). Numerical modeling of dynamic soil-pile-structure interaction, *M.S. Thesis*, Washington State Univ., Pullman, Washington, 126 pp.

Bardet, J. P., and T. Tobita (2001). *NERA: A Computer Program for Nonlinear Earthquake Site Response Analysis of Layered Soil Deposits*, Dept. of Civil Engineering, University of Southern California, Los Angeles, California, 44 pp.

Boore, D. M. (2007). *Some Thoughts on Relating Density to Velocity*, 12 pp., available at http://daveboore.com/daves_notes.php (last accessed October 2014).

Boore, D. M. (2008). TSPP—A collection of FORTRAN programs for processing and manipulating time series, *U.S. Geol. Surv. Open-File Rept. 2008-1111*, 57 pp.

Building Seismic Safety Council (BSSC) (1998). NEHRP recommended provisions for seismic regulations for new buildings and other structures, 1997 edition (FEMA 303), Federal Emergency Management Agency, Washington, D.C.

Dassault Systèmes (2009). *Abaqus Analysis User's Manual, Version 6.9-2*, Providence, Rhode Island.

Dawson, E., W. Roth, and B. Su (2013). 3-D Masing behavior of a parallel Iwan model, in *Challenges and Recent Advances in Geotechnical and Seismic Research and Practice*, J. Hu, J. Ma, J. Meneses, T. Qiu, X. Yu, and X. Zeng (Editors), American Society of Civil Engineers (ASCE) Geotechnical Special Publication No. 232, 549–556.

Dorfmann, A., and R. B. Nelson (1995). Inelastic response of column/girder connections to seismic loads using parallel plasticity, in *Numerical Methods in Structural Mechanics*, J. W. Ju (Editor), Applied Mechanics Division, Vol. 204, American Society of Mechanical Engineers, 13–29.

Elgamal, A., Z. Yang, E. Parra, and A. Ragheb (2003). Modeling of cyclic mobility in saturated cohesionless soils, *Int. J. Plast.* **19,** 883–905.

Fung, Y. C. (1965). *Foundations of Solid Mechanics*, Prentice Hall, Englewood Cliffs, New Jersey, 525 pp.

Hartzell, S., L. F. Bonilla, and R. A. Williams (2004). Prediction of nonlinear soil effects, *Bull. Seismol. Soc. Am.* **94,** 1609–1629.

Hartzell, S., A. Leeds, A. Frankel, R. A. Williams, J. Odum, W. Stephenson, and W. Silva (2002). Simulation of broadband ground motion including nonlinear soil effects for a magnitude 6.5 earthquake on the Seattle fault, Seattle, Washington, *Bull. Seismol. Soc. Am.* **92,** 831–853.

Hashash, Y. M. A., D. R. Groholski, C. A. Phillips, D. Park, and M. Musgrove (2011). *DEEPSOIL 5.0, User Manual and Tutorial*, Univ. of Illinois at Urbana-Champaign, Champaign, Illinois, 107 pp.

Idriss, I. M., and J. I. Sun (1992). *User's Manual for SHAKE91: A Computer Program for Conducting Equivalent Linear Seismic Response Analyses of Horizontally Layered Soil Deposits*, University of California, Davis, California, 37 pp.

Irsyam, M., D. T. Dangkua, Hendriyawan, D. Hoedajanto, B. M. Hutapea, E. K. Kertapati, T. Boen, and M. D. Petersen (2008). Proposed seismic hazard maps of Sumatra and Java islands and microzonation study of Jakarta city, Indonesia, *J. Earth Syst. Sci.* **117,** 865–878.

Ishihara, K. (1996). *Soil Behavior in Earthquake Geotechnics*, Oxford University Press, New York, New York, 350 pp.

Iwan, W. D. (1967). On a class of models for the yielding behavior of continuous and composite systems, *J. Appl. Mech.* **34,** 612–617.

Joyner, W. B. (1977). A FORTRAN program for calculating nonlinear seismic ground response, *U.S. Geol. Surv. Open-File Rept. 77-671*, 50 pp.

Joyner, W. B., and A. T. F. Chen (1975). Calculation of nonlinear ground response in earthquakes, *Bull. Seismol. Soc. Am.* **65,** 1315–1336.

Kaklamanos, J. (2012). Quantifying uncertainty in earthquake site response models using the KiK-net database, *Ph.D. Dissertation*, Tufts University, Medford, Massachusetts, 301 pp.

Kaklamanos, J., L. G. Baise, E. M. Thompson, and L. Dorfmann (2015). Comparison of 1D linear, equivalent-linear, and nonlinear site response models at six KiK-net validation sites, *Soil Dyn. Earthq. Eng.* **69,** 207–219.

Kaklamanos, J., B. A. Bradley, E. M. Thompson, and L. G. Baise (2013). Critical parameters affecting bias and variability in site response analyses using KiK-net downhole array data, *Bull. Seismol. Soc. Am.* **103,** 1733–1749.

Kaklamanos, J., L. Dorfmann, and L. G. Baise (2014). Modeling dynamic site response using the overlay concept, *Geo-Congress 2014 Technical Papers: Geo-Characterization and Modeling for Sustainability*, M. Abu-Farsakh, X. Yu, and L. R. Hoyos (Editors), American Society of Civil Engineers (ASCE) Geotechnical Special Publication No. 234, 1167–1176.

Kwok, A. O. L., J. P. Stewart, Y. M. A. Hashash, N. Matasovic, R. Pyke, Z. Wang, and Z. Yang (2007). Use of exact solutions of wave propagation problems to guide implementation of nonlinear, time-domain ground response analysis routines, *J. Geotech. Geoenv. Eng.* **133,** 1385–1398.

Lee, J.-S., Y.-W. Choo, and D.-S. Kim (2009). A modified parallel Iwan model for cyclic hardening behavior of sand, *Soil Dyn. Earthq. Eng.* **29,** 630–640.

Li, X. S., Z. L. Wang, and C. K. Shen (1992). *SUMDES: A Nonlinear Procedure for Response Analysis of Horizontally-Layered Sites Subjected to Multidirectional Earthquake Loading*, Deptartment of Civil Engineering, University of California, Davis, Davis, California.

Liu, P., R. J. Archuleta, and S. H. Hartzell (2006). Prediction of broadband ground-motion time histories: Hybrid low/high-frequency method with correlated random source parameters, *Bull. Seismol. Soc. Am.* **96,** 2118–2130.

Lysmer, J., and R. L. Kuhlemeyer (1969). Finite dynamic model for infinite media, *J. Eng. Mech. Div.* **95,** 859–877.

Masing, G. (1926). Eigenspannungen and verfertigung beim messing, *Proc. of the 2nd International Congress on Applied Mechanics*, Zurich, Switzerland, 12–17 September 1926 (in German).

Matasović, N., and G. A. Ordóñez (2010). D-MOD2000: A computer program for seismic response analysis of horizontally layered soil deposits, earthfill dams, and solid waste landfills, *User's Manual*, GeoMotions, LLC, Lacey, Washington, 182 pp.

Matasović, N., and M. Vucetic (1993). Cyclic characterization of liquefiable sands, *J. Geotech. Eng.* **119,** 1805–1822.

Matasović, N., and M. Vucetic (1995). Generalized cyclic-degradation-pore-pressure generation model for clays, *J. Geotech. Eng.* **121,** 33–42.

McKenna, F., and G. L. Fenves (2001). *The OpenSees Command Language Manual, Version 1.2*, Pacific Earthquake Engineering Research Center, University of California, Berkeley, California, available at http://opensees.berkeley.edu (last accessed October 2014).

Mroz, Z. (1967). On the description of anisotropic workhardening, *J. Mech. Phys. Solids* **15,** 163–175.

Nelson, R. B., and A. Dorfmann (1995). Parallel elasto-plastic models of inelastic material behavior, *J. Eng. Mech.* **121,** 1089–1097.

Nielsen, A. H. (2006). Absorbing boundary conditions for seismic analysis in ABAQUS, *Proc. of the 2006 ABAQUS Users' Conference*, Cambridge, Massachusetts, 23–25 May 2006.

Okada, Y., K. Kasahara, S. Hori, K. Obara, S. Sekiguchi, H. Fujiwara, and A. Yamamoto (2004). Recent progress of seismic observations networks in Japan—Hi-net, F-net, K-net and KiK-net, *Earth Planets Space* **56,** xv–xxviii.

Ordóñez, G. A. (2010). SHAKE2000: A computer program for the 1-D analysis of geotechnical earthquake engineering problems, *User's Manual*, GeoMotions, LLC, Lacey, Washington, 262 pp.

Parra, E. (1996). Numerical modeling of liquefaction and lateral ground deformation including cyclic mobility and dilation response in soil systems, *Ph.D. Dissertation*, Department of Civil Engineering, Rensselaer Polytechnic Institute, Troy, New York.

Phillips, C., and Y. M. A. Hashash (2009). Damping formulation for nonlinear 1D site response analyses, *Soil Dyn. Earthq. Eng.* **29,** 1143–1158.

Psarropoulos, P. N. (2009). Local site effects and seismic response of bridges, in *Coupled Site and Soil-Structure Interaction Effects with Application to Seismic Risk Mitigation (NATO Science for Peace and Security Series C: Environmental Security)*, T. Schanz and R. Iankov (Editors), Springer, Dordrecht, The Netherlands, 330 pp.

Pyke, R. M. (2000). *TESS: A Computer Program for Nonlinear Ground Response Analyses*, TAGA Engineering Systems and Software, Lafayette, California.

Ragheb, A. M. (1994). Numerical analysis of seismically induced deformations in saturated granular soil strata, *Ph.D. Dissertation*, Department of Civil Engineering, Rensselaer Polytechnic Institute, Troy, New York.

Rayleigh, J. W. S., and R. B. Lindsay (1945). *The Theory of Sound*, Dover Publications, New York, New York, 885 pp.

Reyes, D. K., A. Rodriguez-Marek, and A. Lizcano (2009). A hypoplastic model for site response analysis, *Soil Dyn. Earthq. Eng.* **29,** 173–184.

Sandron, D., L. Sirovich, and F. Pettenati (2011). Near-field response of a 1D-structure alluvial site, *Bull. Seismol. Soc. Am.* **101,** 2981–2997.

Schnabel, P. B., J. Lysmer, and H. B. Seed (1972). SHAKE: A computer program for earthquake response analysis of horizontally layered sites, *Report UCB/EERC-72/12*, Earthquake Engineering Research Center, University of California, Berkeley, 102 pp.

Sincraian, M. V., and C. S. Oliviera (2001). A 2-D sensitivity study of the dynamic behavior of a volcanic hill in the Azores Islands: Comparison with 1-D and 3-D models, *Pure Appl. Geophys.* **158,** 2431–2450.

Thompson, E. M., L. G. Baise, R. E. Kayen, and B. B. Guzina (2009). Impediments to predicting site response: Seismic property estimation and modeling simplifications, *Bull. Seismol. Soc. Am.* **99,** 2927–2949.

Thompson, E. M., L. G. Baise, Y. Tanaka, and R. E. Kayen (2012). A taxonomy of site response complexity, *Soil Dyn. Earthq. Eng.* **41,** 32–43.

Yang, Z. (2000). Numerical modeling of earthquake site response including dilation and liquefaction, *Ph.D. Thesis*, Deptartment of Civil Engineering and Engineering Mechanics, Columbia University, New York City, New York.

Zhang, J., R. D. Andrus, and C. H. Juang (2005). Normalized shear modulus and material damping ratio relationships, *J. Geotech. Geoenviron. Eng.* **131,** 453–464.

***James Kaklamanos*[1]**
Luis Dorfmann
Laurie G. Baise
Department of Civil and Environmental Engineering
Tufts University
113 Anderson Hall
Medford, Massachusetts 02155 U.S.A.
kaklamanosJ@merrimack.edu
luis.dorfmann@tufts.edu
laurie.baise@tufts.edu

Published Online 28 January 2015

[1] Now at Department of Civil and Mechanical Engineering, Merrimack College, 315 Turnpike Street, North Andover, Massachusetts 01845 U.S.A.